

Field Data Observations for Monitoring the Impact of Typhoon "In-fa" on Dynamic Performances of Mono-pile Offshore Wind Turbines: A Novel Systematic Study

Fushun Liu^{a,b,*}, Qianxiang Yu^a, Hongyou Li^c, Yi Zhan^c, Hu Zhou^d, Dianzi Liu^e

^aCollege of Engineering, Ocean University of China, Qingdao 266100, China

^bShandong Province Key Laboratory of Ocean Engineering, Ocean University of China, Qingdao 266100, China

^cJiangsu Guangheng New Energy Corporation Limited, China Green Development Group, Nantong, 210008, China

^dPower China Huadong Engineering Corporation Limited, Hangzhou, 311122, China

^eSchool of Engineering, University of East Anglia, Norwich, NR14 7TH, United Kingdom

Abstract

For offshore structures such as offshore wind turbines (OWT), typhoon is usually considered one of the most critical threats to structural safety performances and service life due to its heavy wind, wave, and even coexisted storm surge. Meanwhile, it is challenging to obtain the systematic data from the environmental conditions, structural dynamic vibrations and the SCADA record, when typhoon passes by the offshore wind farm. Taking into account these situations, a real-time multi-source monitoring system enabling the investigation of the typhoon impact on the performances of OWT, has been firstly established and implemented to a 4.0 MW mono-pile OWT in Rudong, Jiangsu, China. One of the major contributions in this work is to develop the monitoring system using a unique environment of real-world data that has been synchronously obtained from waves, winds, vibrational accelerations, inclinations of towers and SCADA data during the typhoon "In-fa" passing by the wind farm, and provide the scientific community with the underlying standards and technical recommendations. To investigate the influence caused by "In-fa", comparison results of the measured data in the range of June to August have been analysed. It is worth noting that two conclusions have been obtained: 1) the region near the nacelle is not always the most critical vibrational area. Actually, the change of the maximum structural response in the position under different external loads should be applied to effectively evaluate the structural safety; 2) the measured accelerations exhibit an obvious decay process in the presence of the turbine rotor-stop, but not the yaw rigid-body motion. This observation promotes the accurate identification of modal parameters for the long-term monitoring. Consequently, these valuable findings to facilitate the assessment of structural operational conditions have been developed into two guide-lines. All the data and analyses presented in this paper provide a valuable insight into the design, energy efficiency, safety monitoring and damage diagnosis of OWT structures.

Keywords:

Offshore wind turbine, typhoon "In-fa", multi-source monitoring system, field measured data, dynamic performance

1. Introduction

Supporting structure is one of the most important components of OWT and determines its service life. In the long-span operational period, the supporting structure is always threatened by the complex and harsh ocean environments including heavy wind, waves, and extreme situations like typhoons, which would cause serious fatigue or damage or even collapse. The structure monitoring system is one of the most effective ways to mitigate these possible attacks. A systematic monitoring system can not only reduce potential hazards but also provide effective data resources for the delicate analysis and optimization of the structure under complex environmental conditions. However, the application of a systematic monitoring system for OWTs is always a particularly challenging task with the difficulties of installation, data sharing and communication, long-term operational reliability and maintenance. Most of the OWT structure monitoring systems work on single-source data that only includes the vibrational acceleration, inclination, displacement or strain [1–4]. Furthermore, limited by the field infrastructures such as power supply or network coverage, some of the field tests do not have the capability of the long-term and continuous monitoring and recording the complete operational cycle. Therefore, the analysis mainly focused on the traditional modal analysis [5–10]. In fact, the structure response and status are closely related to environmental and operational conditions, for example, the nacelle vibration produces extra harmonic components and the second-order mode is more sensitive to the water level [11–14]. In particular, under extreme load conditions such as typhoon, the more severe marine climatic conditions will cause stronger structural vibration and displacement, which brings greater potential safety hazards to the structural integrity.

Typhoon is one of the most serious threats to the safety of wind turbines (WTs) according to the statistics of "Caithness windfarm Information Forum" [15] from 1998 to 2020 as shown in Table 1. The detailed information of statistical accidents are shown in appendix A1. In these accidents, most of them are structural failures, besides a few blade damage and transmission damage [16] such as shown in Fig. 1. As compared with other types of accidents, consequences caused by typhoon are more serious. Thus, it is

*Corresponding author.

Email address: percyliu@ouc.edu.cn (Fushun Liu)

of great importance to monitor and analyse the response state and the possible impact during the typhoon period. Therefore, the typhoon related research on WTs, such as mechanism studies, accidents, design reliability and extreme load effect analyses, has been extensively conducted [17]. In terms of mechanism study, most of the researchers utilized the measured typhoon parameters (wind speed and direction, etc.) to generate a numerical model by CFD, FAST or IMF for the prediction of the responses of interests under the extreme loads and investigate the changes of structural vibration characteristics caused by other different load conditions [18–25]. Koji et al. compared numerical results with the field measured data to verify the effectiveness of the simulated model [26]. In terms of accident analysis, Takeshi et al. analyzed a structure damage scenario caused by typhoon MAEMI in Miyakojima island wind farm of Japan in 2003 [16]. The maximum gust wind speed of the typhoon reached 74.1 m/s, resulting in serious accidents such as blade breaking and tower collapse. In 2013, Zheng et al. studied several wind turbine failures caused by Typhoon Saomai in the Hedingshan wind farm of Zhejiang Province, China, in 2006. Results showed that the violent wind, drastic turbulence and sudden change in the wind direction were the major factors leading to wind turbine failures [27]. In 2015, Chen et al. conducted the failure analysis in wind turbine accidents caused by Typhoon Dujuan (2003) and Usagi (2013), respectively. It was noted that both extreme winds and the stop positions of WTs were critical factors in the failure progress of turbines due to the change in wind direction during the typhoon impact. Moreover, the dramatic thinning of the shell wall due to possible design defects was also identified as the source of the tower collapse [28] [29]. In terms of typhoon design reliability, Tang et al. used static strength theories to calculate the response parameters of the WTs structure under strong wind conditions, and further, to optimize and improve the WTs structure's anti-typhoon ability of WTs [30]. Chi et al. studied the typhoon impacts on the foundation design of offshore wind turbines [31]. In terms of extreme load effect studies, Lin and Li et al. investigated the extreme load effects on the structural response of an offshore wind turbine jacket foundation under typhoon conditions [32–34]. Huang et al. analysed the damage probability of mono-pile OWT under action of typhoon [35]. And Qin et al. presented a DTU 10 MW mono-pile OWT numerical model to research the dynamic characteristics under typhoon. The results showed that pitch control of blades can effectively reduce the wind loads and the dynamic load under the base is obviously affected by wave load and wind load [36].

Table 1: Statistic of wind turbine accident and incident with typhoon hurricane [15].

Accident Type	Total Amount	Date
Structural failure	14	1998-2020
Blade failure	3	2005,2007,2013,2019
Transport	1	2007
Miscellaneous	1	2017

*See Appendix for details.



Fig. 1: Typhoon caused structure accidents of WT: (a) tower collapse, (b) blades failure [16].

In recent years, OWTs have developed rapidly and gradually replaced onshore WTs as the main growth in the exploitation of wind energy resources. As compared with onshore WTs, the surrounding environment of OWTs is more complex and adverse. OWTs may sustain not only the heavy wind load, but the strong wave, current, seawater and salt spray corrosion. In particular, the foundation and tower structure subject to the typhoons have to bear the combined actions of the extreme wind, wave and current loads, under which the structure is easily prone to fatigue and damage. Therefore, the study on typhoon-induced risks to structural safety of OWTs is more worthy and valuable [37]. In 2019, Sun et al. carried out the field measurement research on structural vibration and tilt of a high-rise pile cap supporting foundation in batholith seabed under the action of typhoon Meranti, South China Sea. Results showed that the typhoon significantly affected the vibration and instantaneous tilt of the supporting system, however it had a slight impact on the first natural frequency. Also, rock socketed pipes performs better than driven frictional pipes in terms of resistance to the vibration and tilt [38]. At the same time, Dong et al. proposed a comparison

analysis of vibrational response characteristics of a prototype of OWTs subject to three different typhoons in a sea area of Jiangsu, China. It was observed that the change of rotor speed and yaw rigid-body motion had the more obvious impact on the structural vibration than the variation of wind speed [39–41]. In 2020, Huadong Engineering Corporation Limited and other units jointly carried out a number of typhoon-induced strong vibration analyses of the single pile and high-pile-concrete OWTs. At present, there are few research studies focusing on the field measured data from OWTs during typhoon passage. The main reason is that data from the long-term monitoring system of OWTs structure is hardly captured due to the random passage of typhoons. Moreover, influences of the typhoon on structural responses of OWTs are induced by multi-sources which have obvious coupling and correlation effects. Undoubtedly, the study on multi-source data comparison and correlated analysis for a more accurate and comprehensive conclusion is attracting more attention as the scarcity and preciousness of field multi-source data are realized [42].

Taking into account the aforementioned situations, a real-time multi-source monitoring system has been first established to conduct a comprehensive study on a 4.0 MW mono-pile OWT in Rudong, Jiangsu Province, China. As the typhoon "In-fa" passed through, the monitored wind farm on July 24th-29th, 2021, a systematic data analysis and comparison have been presented to investigate the impact of the typhoon on the environment, structural responses and operational conditions. Also, the study will provide a valuable insight into the design, safety monitoring, and damage diagnosis for the OWT structures under extreme loads. The article mainly consists of the following parts: Section 2 introduces the basic information of the monitoring system including wind farm location, monitoring contents and field situations; Section 3 presents a systematic comparative analysis and integrity evaluation of the OWT structure subject to the typhoon impact; Section 4 mainly describes two valuable findings - the most serious vibrational position under different external loads and the decay response when the rotor-stop occurred and Section 5 concludes the whole contents and results of the research.

2. Establishment of a Monitoring System on a 4.0 MW Mono-pile OWT

Towards a multi-source structural monitoring system for OWTs will play a significant role in the damage detection and condition assessment. It is estimated that by the end of 2021, China will become the country with the largest installed capacity of offshore wind power [43]. However, with the rapid development of OWT industry, only a few systematic monitoring systems have been put into operation in domestic [44]. As most of the structure monitoring systems only record vibrational responses, the related environmental

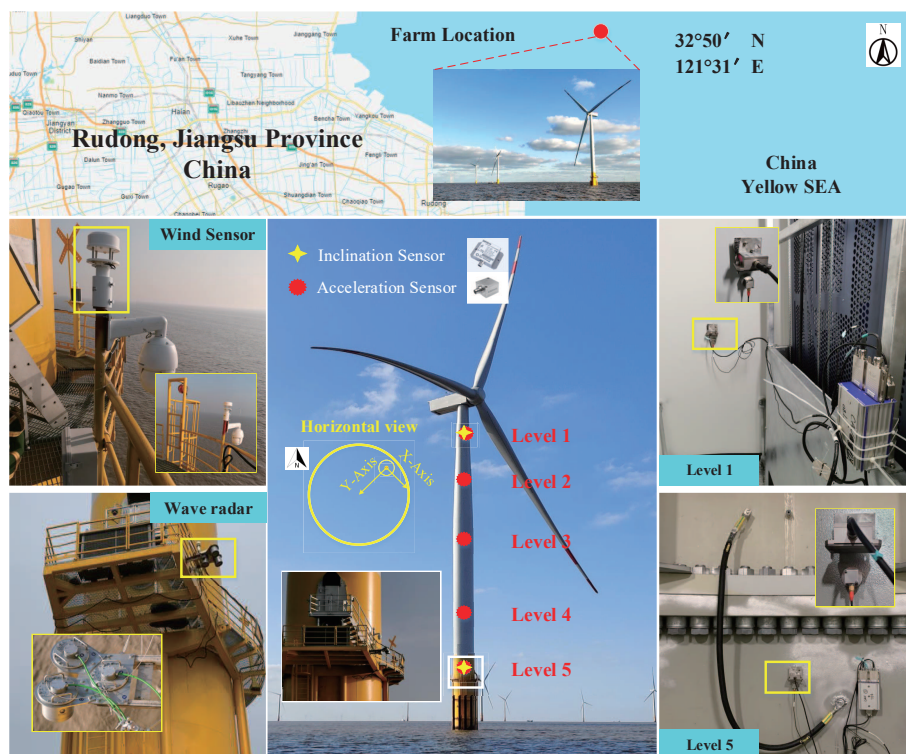


Fig. 2: Wind farm location and monitoring system.

and operational parameters are barely included. This greatly limits the applications and ability of structural condition analysis.

To address this issue, this paper will introduce a real-time multi-sourced structure monitoring system that has been established on a 4.0 MW mono-pile OWT in Rudong, Jiangsu, China. It is expected to provide a systematic reference scheme and data support for the construction of OWTs with the underlying standards and technical recommendations. The selected wind farm is located at about 44 km off the coast in Rudong owned by CGDG (China Green Development Group). It is composed of fifty 4.0 MW mono-pile wind turbines, leading to a total of 200 MW power output capacities. The monitoring system is established on the 37# OWT. The wind farm officially operated and connected to the grid in December 2020, and the monitoring system is deployed in January 2021 to provide a more valuable reference and more complete data resource for future studies. The wind farm location and monitoring system in the field are shown in Fig. 2. The content of the proposed system consists of three modules: **Environment**, **Structural response** and **Operational condition**. The environment part is realized by a wave radar and two wind sensors installed on the edge of the outer platform. The diagrammatic sketch of wave measurement has been demonstrated in Fig. 3. The wave radar is an optional component in the structure condition monitoring system, while the wave

load is an indispensable part of the structural response, especially during the typhoon period. Therefore, the implementation of the wave radar empowers the proposed system with the capability of monitoring the wave data. It is worth noting that only the water elevation is directly measured by wave radar, other parameters related to wave are derived from the elevation data. The structural response part contains two types of data: the vibrational acceleration and inclination. The acceleration data is measured by five 3-axis MEMS (Micro Electro Mechanical System) acceleration sensors that are separately mounted on the different heights of the supporting structure with the specifications of 13 meters, 25 meters, 58 meters, 79 meters, 93 meters (the position of operational platform in the tower) from the 1985 national elevation benchmarks. To simplify the notation, the specifications of heights are annotated in the range of Level 5 to Level 1 accordingly. The horizontal view indicates the x-axis (roll) and y-axis (pitch) directions of acceleration (inclination) sensor in Fig. 2. Two inclination and acceleration sensors are installed at Level 1 and Level 5. The operational conditions module acquires the parameters including the rotor speed, nacelle yaw angle and blades pitch angle from the SCADA system, which owns an independent time o'clock and sampling rate. Therefore, the parameters in the operational condition module have been synchronized with data from the other two modules. Sampling rates of the wind and wave are 200 Hz and 10 Hz, respectively. The detailed information about monitoring system including equipment and sensor specifications, amount, measurement information and sampling rate are concluded in Table 2. Moreover, the system has the ability to realize the real-time data synchronization, remote control, power-off protection and self-start-up, therefore it provides a solid foundation for long-term monitoring and system maintenance.

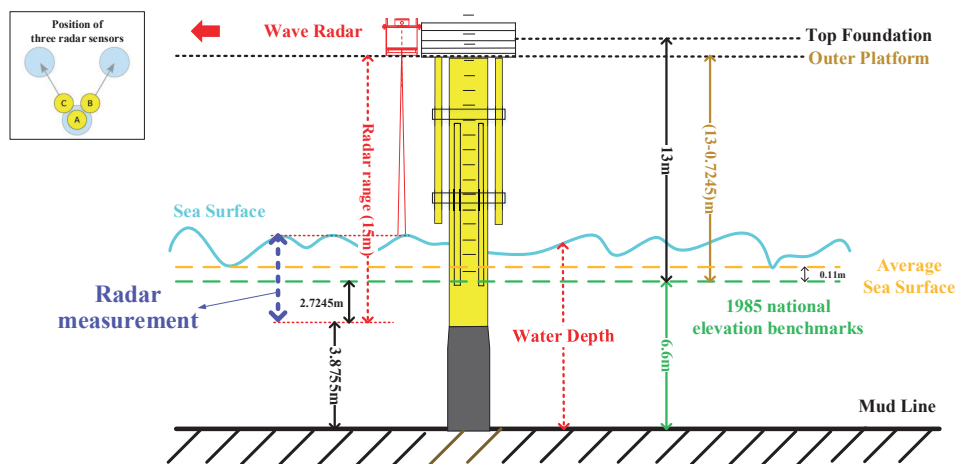


Fig. 3: The diagrammatic sketch of wave radar measurement.

Table 2: The detailed information of monitoring system.

	Equipment & Sensor	Specification	Amount	Measurement	Sampling rate
Environment	Wave radar (Sensor: A,B,C)	RadacWG5 Distance: 2-75 m (± 3 mm) Height: 0-60 m (± 1 cm) Direction: 0-360° ($\pm 2^\circ$) Period: 1-100 s (± 50 ms) Sampling: ≤ 10 Hz	1	Wave height (A) Wave elevations (A,B,C) Wave period (A) Wave direction (B & C)	10 Hz
		RS-CFSFX-N01-2 Speed: 0-60 m/s (± 0.2 m/s) Direction: 0-360° ($\pm 3^\circ$) Sensitivity: 0.01 m/s		2	
Structural response	Acceleration sensor	TE-Model-4835A Dynamic range: ± 2 g Axis: 3 Sensitivity: 1000 mv/g Frequency response: 0-250 Hz	5	Vibration acceleration (3-axis)	200 Hz
		SST810 Range: $\pm 300^\circ$ ($\pm 0.1^\circ$) Direction: $\pm 90^\circ/180^\circ$ Axis: 2 (Pitch & Roll) Sensitivity: 0.05° Sampling rate: ≤ 400 Hz			
Operational condition	SCADA	-	1	Rotor speed Blade pitch Nacelle yaw	0.1 Hz

1* The wave radar has three sensors which independently measure the **wave elevation** data. The wave height and period are derived from the **wave elevation** data by sensor A, and the wave direction is calculated by the measured data from sensor B and C.

2* The direction 0° (or 360°) means north, 90° means east.

3. Impact study of typhoon "In-fa" on the Monitored OWT

Understanding the performance of OWT under the extreme load is very instructive for the structural safety evaluation. To analyze the impact of typhoon "In-fa" on dynamic performances of OWT, three modules including the environment, structure response and the synchronized operational conditions introduced in Section 2 have been studied as follows.

3.1. Basic information of typhoon "In-fa"

Typhoon "In-fa" was the sixth typhoon of the Pacific in 2021. It was first upgraded as a tropical storm by the Central Meteorological Observatory of China at 2:00 on July 18th, 2021, and then a strong typhoon at 11:00 on July 21th. Finally, super typhoon "In-fa" landed in Putuo District, Zhoushan at 12:30 on July 25th and the maximum wind force near the center was observed with the value of 38 m/s. Fig. 4 demonstrates

a four-stage traveling passage of typhoon "In-fa". On July 23th, it was formed from a strong typhoon level to typhoon level at night and the edge of the typhoon circle reached the wind farm location. It landed on the east coast of China on July 25th with the seven-level wind circle affecting the wind farm. On July 26th, it was further weakened into a strong tropical storm with a center wind speed of 28 m/s in the west of Hangzhou Bay. In the early morning of July 28th, it was classified as a tropical depression in Anhui Province.

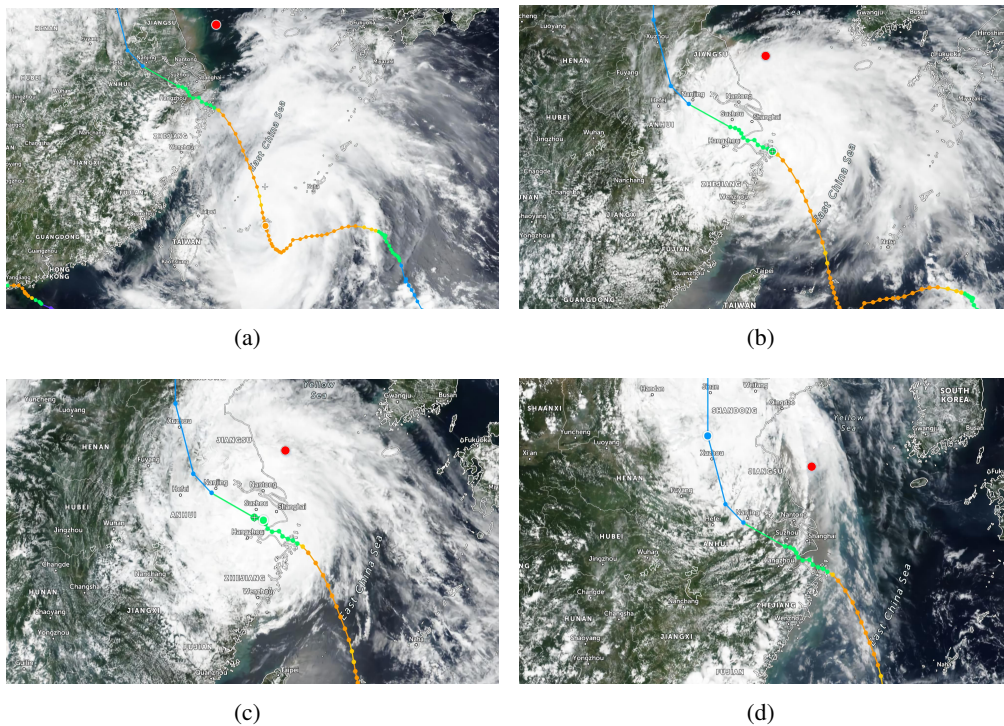


Fig. 4: Schematic diagram of a wind turbine in different typhoon-influenced stages: (a) before landing with 150 km/h at 14:00, July 23th, (b) landing with 100 km/h at 14:00, July 25th, (c) during landing with 65 km/h at 20:00, July 26th, (d) after landing with 45 km/h at 8:00, July 29th [45]

3.2. Investigation on the measured data from typhoon "In-fa" and a comparison with previous records

3.2.1. Environment comparison

Comparison results of the typhoon period (July 24th-29th) and the previous record (June 24th-29th) are studied to demonstrate the impact of the typhoon on the environment. As the characteristics of environment and structural responses are sensitive to the behaviours of the typhoon including the centre latitude, pressure and longitude, environment responses and their correlations are first investigated as follows. It should be noted that both the reference periods of statistical values (mean, maximum, root mean square etc.) of

wind (wind speed and direction) and SCADA are 10 mins. The reference period of waves (height, period and direction) is 1 hour. During July 24th-29th, the typhoon "In-fa" induced strong wind had the maximum instantaneous wind speed of 29.49 m/s at the wind farm. As shown in Fig. 5, the wind speed has significantly increased, as compared with the same period last month. Its average value reached 14.85 m/s, which is higher than the rated wind speed of the turbine. According to the SCADA data, the proportion of the OWT with a full power status reached 94.95% in the whole typhoon period. Fig. 7 describes the wind roses on June 24th-29th and July 24th-29th. It is noted that the wind mainly came from the southwest and northeast in both two periods, but the typhoon induced a stronger north wind than usual. Also, the OWT did not stop as the average wind speed (denoted as the solid red line in Fig. 5) is smaller than the cut-out wind speed.

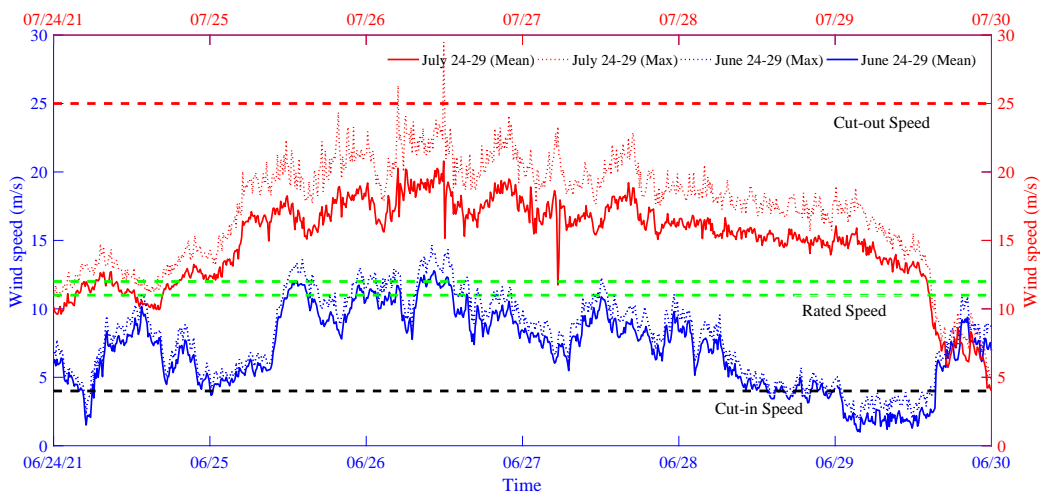


Fig. 5: The comparison of wind speed before and during the typhoon.

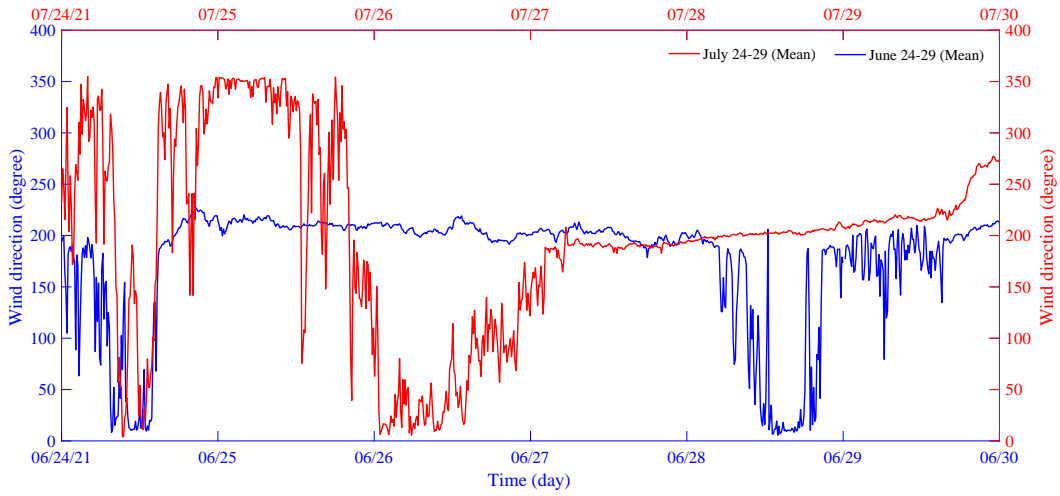


Fig. 6: The comparison of wind direction before and during the typhoon.

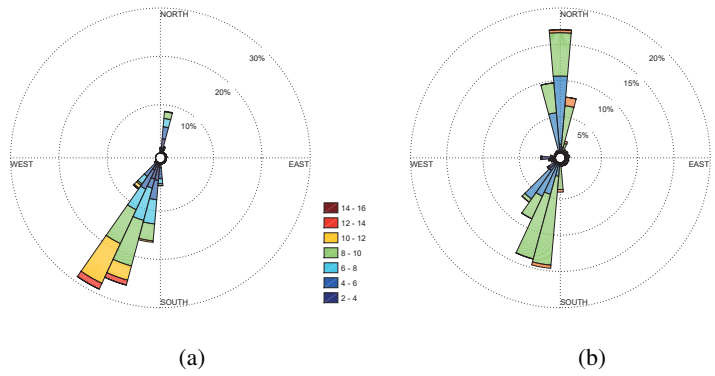
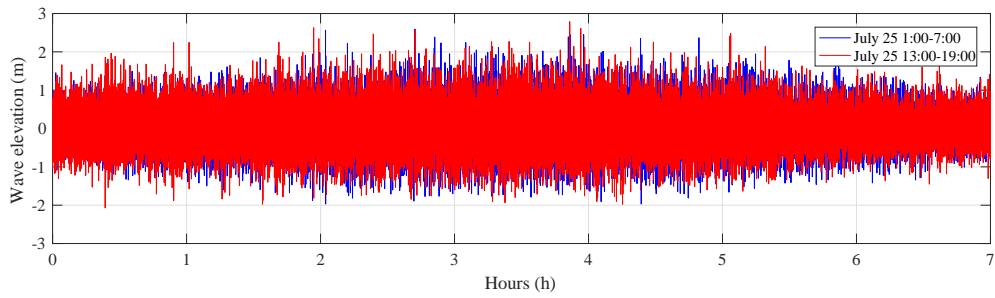
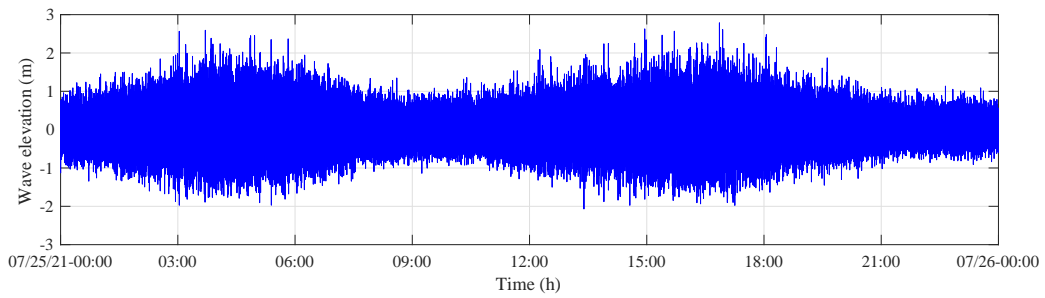


Fig. 7: Wind roses before and during the typhoon: (a) June 24th-29th, (b) July 24th-29th.

Generally, typhoons are not only accompanied by strong winds but waves and surges. Wave condition is one of the most important factors that affect the structural state. To understand the wave changes caused by the typhoon in more details, studies of several wave parameters are conducted as follows. The wave elevation series and original radar measurement on July 25th are presented in Figs. 8 and 9, respectively. It should be noted that the wave elevation data is obtained by the removal of the tidal and DC components of the radar measurement using a high pass filter equipped in each radar sensor. After that, a de-averaging procedure is deployed on the wave elevation data as the small DC component may still be presented in the filtered signal. Therefore, the wave elevation time series have mean value of zero. Meanwhile, it can be observed that the wave elevation values from 01:00-07:00 and 13:00-19:00 are bigger than the rest of time on July 25th. This phenomenon is consistent with the tidal elevation variation in Fig. 9.



(a)



(b)

Fig. 8: Wave elevation: (a) measurement comparison between July 25th, 01:00-07:00 and July 25, 13:00-19:00, (b) 24 hours' data on July 25th.

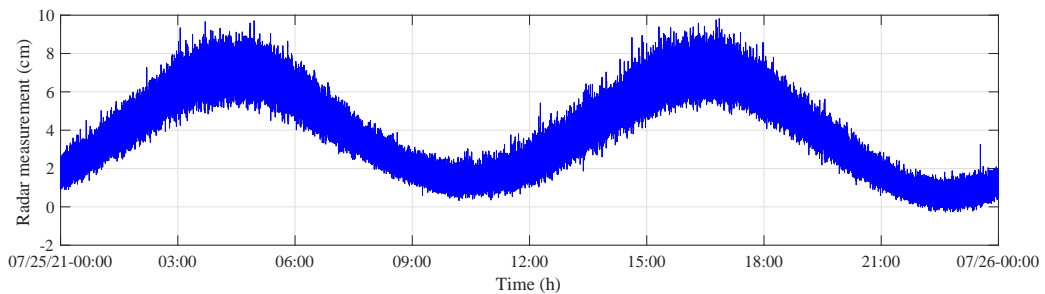


Fig. 9: The original radar measurement on July 25th.

Three wave height indexes including the maximum wave height, the significant wave height and the mean wave height which derived from the wave elevation data, are presented in Fig. 10. In June, the wave heights kept stationary progress with the maximum value of 2.156 meters. Before the typhoon landing, the change in wave heights in the first half of July was the same as that in the first half of June. After the typhoon reached the wind farm, the wave height had gradually accumulated since July 20th. During the typhoon period, the maximum wave height was achieved with the highest point 4.276 meters on July 25th, which is more than two times larger than the maximal wave height in June. More specifically, as compared

with the data in two periods before the typhoon shown in Fig. 11a and b, the distribution of wave heights during the typhoon in Fig. 11c was mainly reflected by the components with wave heights larger than 1-1.5 meters. As shown in Fig. 11c, the wave height was significantly increased during the typhoon, while the wave height of 1-1.5 meters was hardly observed during the non-typhoon period. However, more than 50% of the wave height was still distributed in the range of 0-1 meters, so the overall distribution shape of wave height did not change greatly.

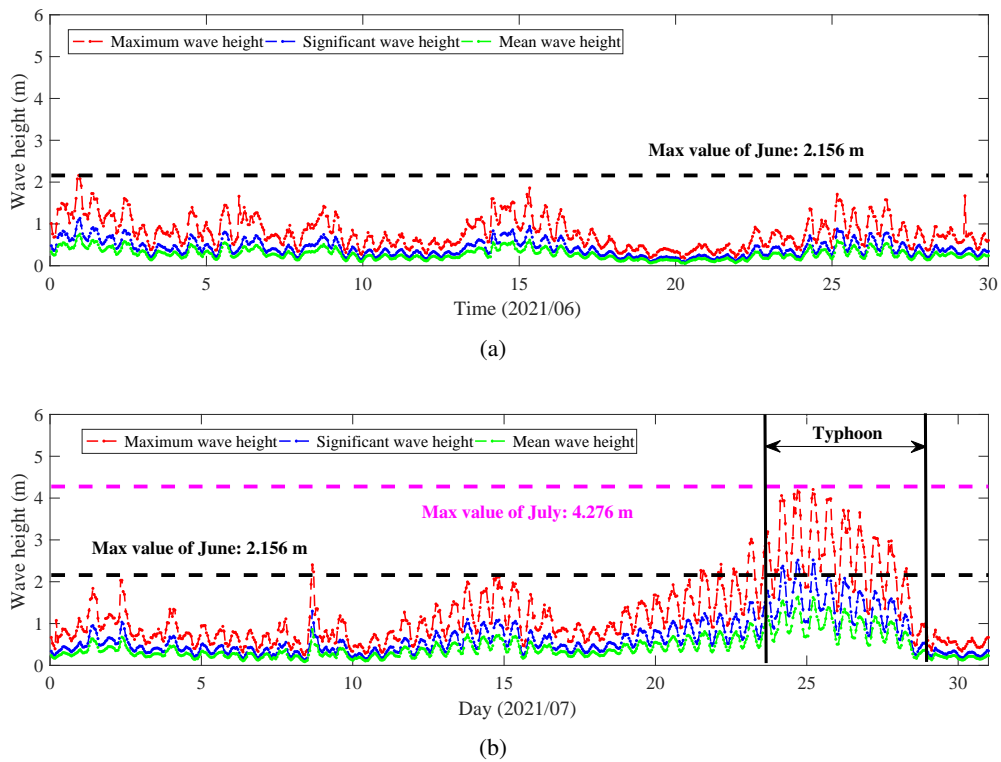


Fig. 10: Wave height: (a) June, (b) July.

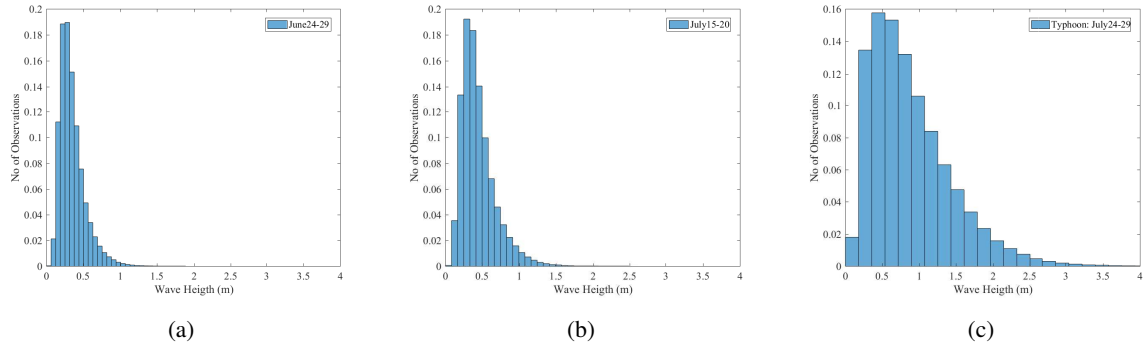


Fig. 11: Wave height statistical histogram: (a) June 24th-29th, (b) July 15th-20th, (c) July 24th-29th.

Generally speaking, the typhoon significantly will cause affects the tide level in the sea area where it passes to rise significantly. As shown in Fig. 12, the tide level during the typhoon has already passed the design high level (3.15 meters) on July 24th-28th, and its maximal value reached at 4.3764 meters. However, it did not exceed the extreme high level (4.98 meters). After July 28th, the tide level gradually dropped below the design high level. Though the typhoon led to the great changes in wave characteristics of the great wave changes, its significant wave height and period did not exceed the design values of 50-year return period, which were 11.19 s and 4.5 meters and 11.19 s, respectively. It is worth noting that the remarkable change of the wave height occurred on July 25th and wave period on July 26th.

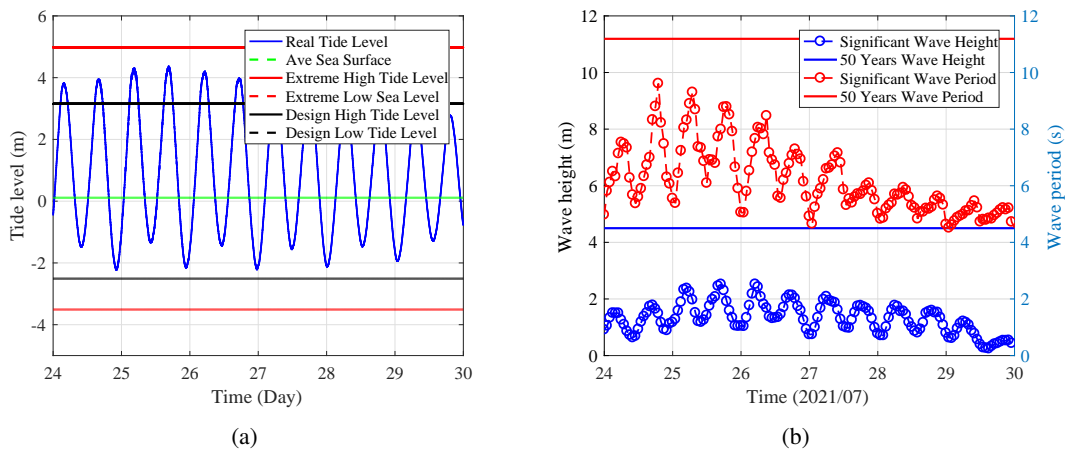


Fig. 12: Tide level and wave height condition during the typhoon: (a) tide level, (b) significant wave height and period.

3.2.2. operational condition

Rotor speed is an important and representative parameters in SCADA system that reflects the operational condition of the turbine. As mentioned above, in Section 3.2.1, typhoon "In-fa" resulted in bringing more severe environmental conditions, especially the strong wind which is inevitably leads to a faster rotor speed. In the service-life of OWT structures, the wind speed and rotor speed are the two major factors that have a significant impact on the structural responses. The wind and rotor speed specifications of the monitoring turbine are shown in Table 3. When the wind speed is [0-3] m/s, the wind turbine is in the parking state and the rotor speed is about 0 r/min. When the wind speed increases to 10.2 m/s, the wind turbine works in the rated state and the rotor speed keeps at [10.9-12.9] r/min. When the wind speed is over 25 m/s, the wind turbine cuts out and turbine stops rotating.

Table 3: The operational parameters: wind and rotor speed.

Rotor speed range (r/min)	Wind speed (m/s)		
	Cut-in	Rated	Cut-out
0-12.9	3	10.2	25

In the proposed monitoring system of this paper, data from the environment, the SCADA and structural responses were synchronously collected. The synchronized data of the acceleration, rotor speed and wind speed presented in Fig. 13 to demonstrate their correlations. The turbine rotor switched between the operational and parking status led to the change in wind speed on June 29th in Fig. 13a. When the start-up of the rotor happened, the structural acceleration response significantly increased as the wind speed increased in operation conditions. Also, the amplitude was approximate 0.01g (1 g=9.8 m/s^2) in the parking state. After start-up, the acceleration amplitude increased 1-1.5 times. During the typhoon, the data was given in Fig. 13b on July 26th. It can be observed that the rotor speed kept at 10-11 r/min which is defined as the rated rotor speed. There were a few short intervals, where sudden drops of the wind speed and the rotor speed were observed. The acceleration amplitude in the rated rotor speed period was more than two times larger than the value on June 29th. In summary, as the envelope curves of the acceleration, rotor speed and wind speed agree well, the vibrational intensity is clearly proportional to the combination of the wind speed and rotor speed. As shown in Fig. 13, the maximum values of acceleration, wind speed and rotor speed before and during the typhoon were 0.0483 g, 10.8 m/s, 11.3 r/min and 0.2045 g, 29.49 m/s, 11.6 r/min,

respectively. The average wind speeds in these two periods were 3.95 m/s and 18.11 m/s.

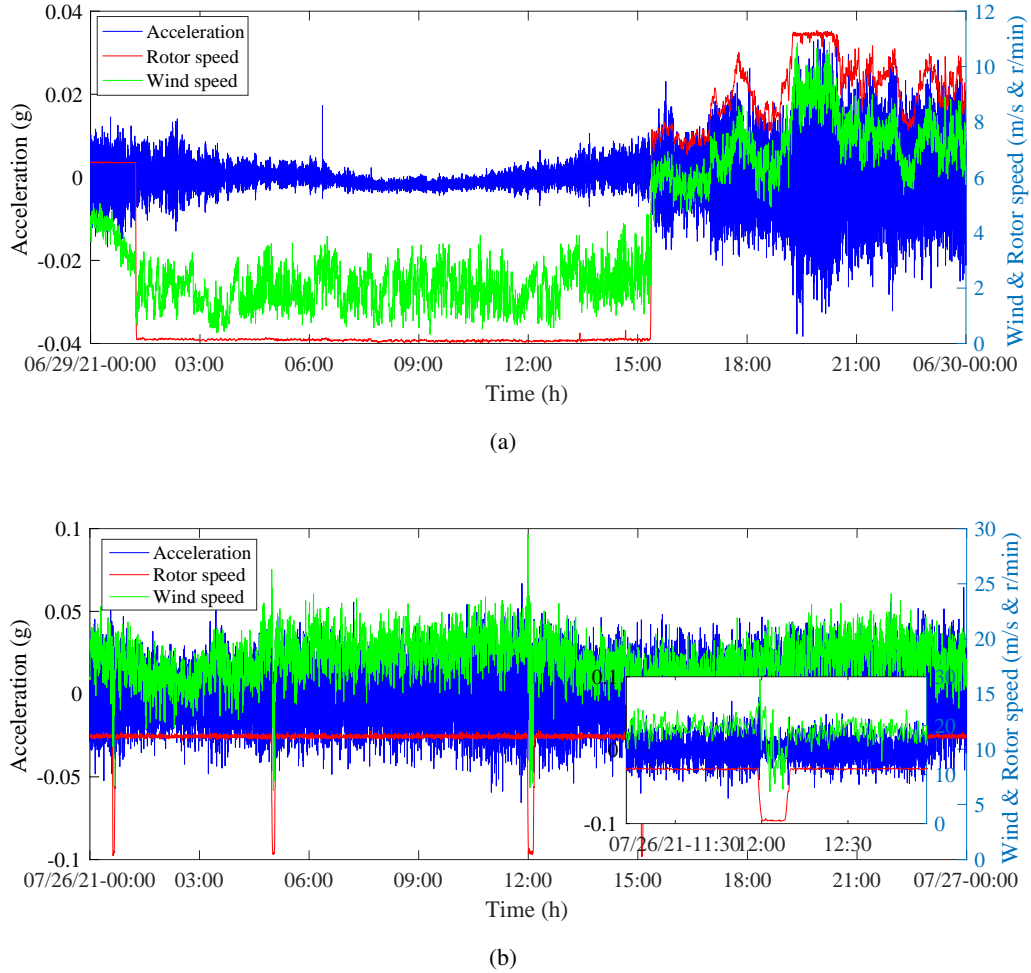


Fig. 13: Synchronized relationship among acceleration, wind speed and rotor speed: (a) before the typhoon, (b) during the typhoon.

3.2.3. Structural responses

The comparison results of vibrational acceleration and inclination signals between the typhoon period and previous record were shown in Figs. 14 and 15. The structural response data (including acceleration and inclination) information presented in this paper was collected under the normal turbine operation. That means the turbine operational modes would adaptively switched with the wind speed variation. The sampling rates of acceleration and inclination are 200 Hz and 10 Hz, respectively. The reference period of statistical values of structural response (acceleration and inclination) is 10 mins. Sensors at two levels (Levels 1 and 5) were selected to demonstrate the changes induced by the typhoon. During the typhoon period, the maximum instantaneous acceleration value reached 0.2045 g, which is two times larger than the value

of 0.0858 g obtained on June 24th-29th. At Level 1, the maximum vibrational accelerations were 0.0395 g and 0.0737 g before and during the typhoon, respectively. The similar conclusion could be drawn based on the data from the sensor at Level 5. Meanwhile, the changes in structure inclination were shown in Fig. 15. During the typhoon period, the maximum instantaneous inclination value at Level 1 was 1.3602 degrees, as compared with 0.9974 degrees on June 24th-29th. At Level 5, the maximum instantaneous inclination were 0.2408 degrees and 0.3411 degrees before and during the typhoon, respectively.

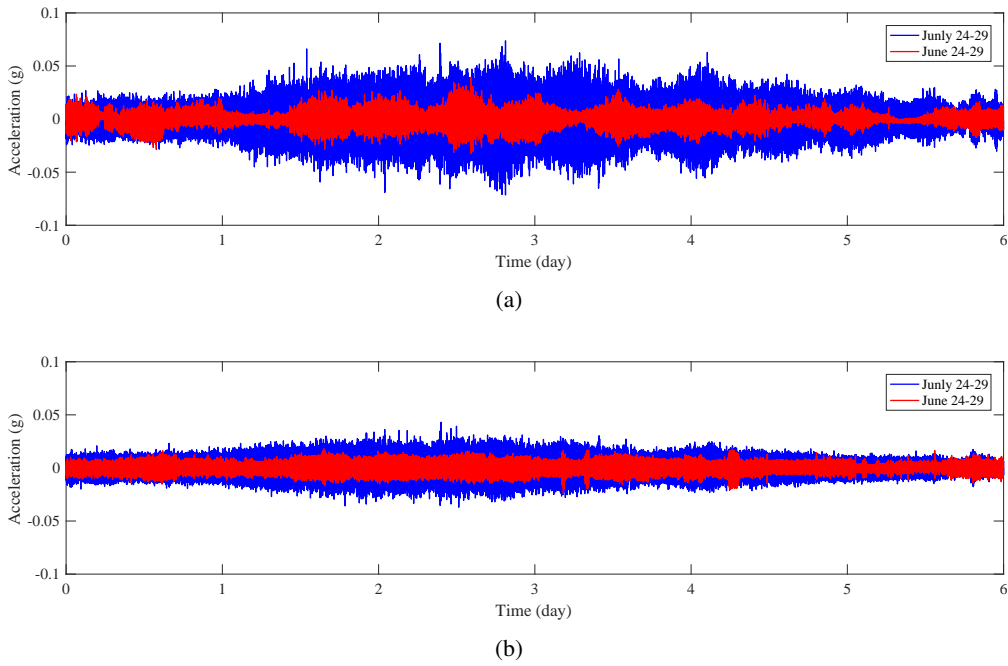


Fig. 14: Acceleration comparison (down sampling to 10 Hz): (a) Level 1 y-axis, (b) Level 5 y-axis.

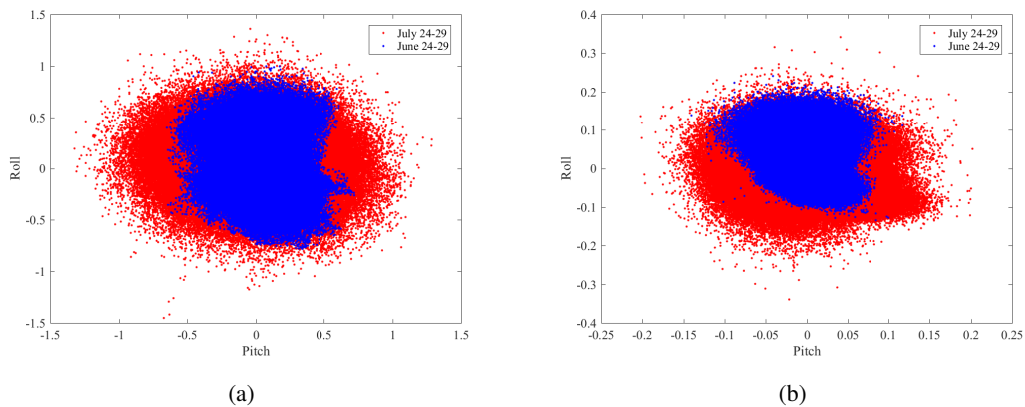


Fig. 15: Inclination comparison: (a) Level 1 (tower top), (b) Level 5 (tower bottom).

During the typhoon, the dominant wind mainly includes the southwest or northeast wind direction, which is close to the pitch direction of the inclination. This agreement can be represented in the form of the elliptical distribution of the inclination data with the pitch and roll directions along the long and short axes, respectively. As the wind speed is the main factor affecting the structural response, the relationship between the wind speed and acceleration RMS (Root Mean Square) can be decomposed into four stages shown in Fig. 16. Stage I: when the wind speed is lower than the cut-in wind speed, the structural response fluctuates in a small range, and the amplitude is less than 0.005 g; The second stage is when the wind speed is between the cut-in wind speed and the rated wind speed, the acceleration amplitude is linearly proportional to the wind speed, and the maximum RMS value is about 0.01 g. In this stage, the rotor speed is gradually increasing along with the wind speed and the three blades are keeping at maximum upwind angle consistently. The third stage is when the wind speed is higher than the rated wind speed, but smaller than 15 m/s, the acceleration decreases with the increase of the wind speed. This phenomenon is mainly induced by the pitch controlling operation of reducing the windward angle as the wind speed exceeds the rated wind speed (10-11 m/s). It should be noted that the impaction induced by typhoon is mainly demonstrated in Stage IV: When the wind speed exceeds 15 m/s, the acceleration is linearly proportional to the wind speed as the relationship in Stage II. When the wind speed is about 20 m/s, the acceleration RMS value is about 0.015 g. Meanwhile, the acceleration RMS as a two dimensional functions of wind speed and significant wave height are presented in Fig. 17. As shown in Fig. 17, the significant wave height is positively related to the structural response intensity. And the distribution of wave height data during typhoon period can be clearly distinguished from that during the same period in June. Although the contribution of wave height to structural vibration is lower than that of wind and operational conditions, the strong coupling relationship between wind and wave also leads to a positive relationship between wave height and structural vibration.

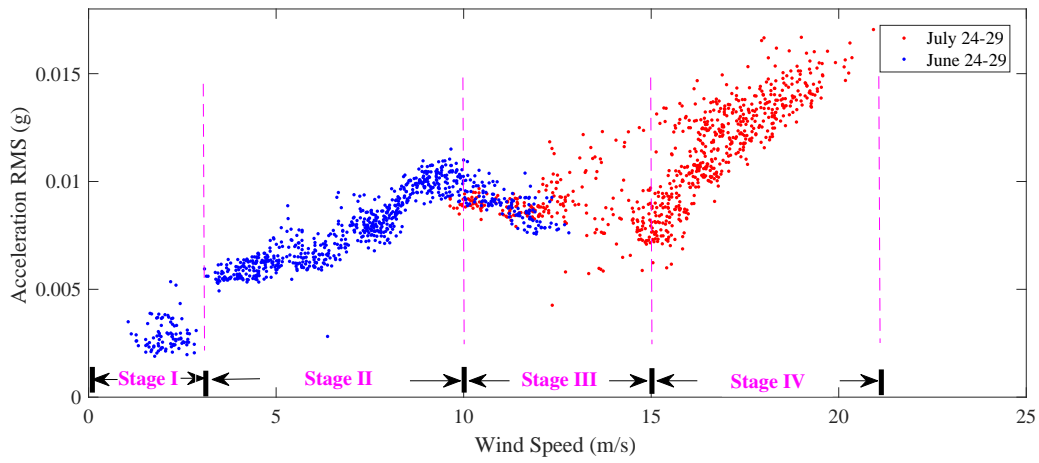


Fig. 16: The relation between wind speed and acceleration RMS.

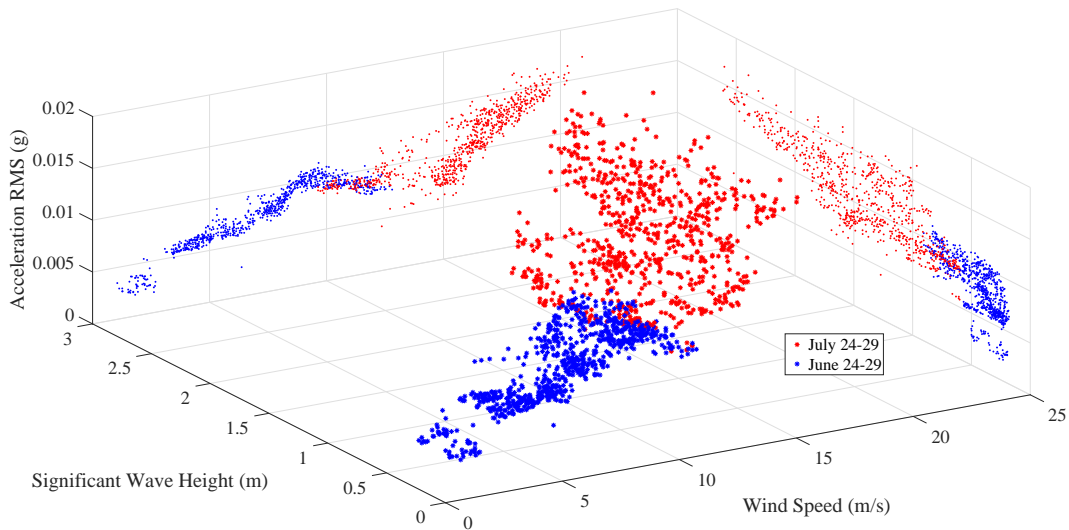


Fig. 17: The acceleration RMS related to wind speed and significant wave height.

To further investigate the impact of typhoon "In-fa" on the monitoring OWT, the maximum values of environmental and structural responses during the typhoon have been given in Table 4. These results provide an effective index for the evaluation of OWT condition states. It can be observed that the typhoon transit leads to a remarkable increase in the amplitudes of environmental and structural responses.

Table 4: The maximum values of environment and structural response data.

	Wind Speed (m/s)		Wave (m)		Acceleration (g)		Inclination (deg)	
	RMS	Instant	Wave height	Tide level	RMS	Instant	RMS	Instant
	(10 mins)				(10 mins)		(10 mins)	
June 24 th -29 th	12.80	14.67	1.71	3.49	0.016	0.085	0.5651	1.59
July 15 th -20 th	14.04	16.45	2.11	2.98	0.019	0.076	0.545	1.34
July 24th-29th (Typhoon)	20.92	29.49	4.27	4.37	0.024	0.204	0.796	2.76

Moreover, Zhang et al. [40] concluded that the yaw rigid-body motion of nacelle can excite strong tower vibrations and further cause the potential structural fatigue in the long operation service. Therefore, the proportion of four ranges of instantaneous yaw angle have been studied in Table 5. It is noted that the proportion of the larger instantaneous yaw rigid-body motion has been significantly increased during the typhoon, especially for the yaw angle larger than 100 degrees.

Table 5: The proportional statistics of instantaneous nacelle yaw rigid-body motion.

	[0, 20]		[20, 50]		[50, 100]		>100		Total
	Amount	Ratio	Amount	Ratio	Amount	Ratio	Amount	Ratio	Amount
June	245669	95%	5896	1.5%	3959	1.4%	3673	2.1%	259200
July	247807	92%	10716	2%	3991	2%	5325	4%	267840
July 24th-29th (Typhoon)	43417	83%	4822	2.5%	1326	4.3%	2274	9.2%	51840

In summary, the monitored responses and indicators have been increased to a great extent during the typhoon, as compared with the previous records. It is worth noting that in the whole process of typhoon-induced impact, the OWT does not stop as the average wind speed that is used as a criterion for the evaluation of the parking state, does not surpass the cut-out wind speed. Also, the rated speed has been maintained for power generation for a long time, and the full power generation rate has been significantly improved. As the long-term sustained large vibration caused by the typhoon inevitably affect the responses of OWT structures, statistical analysis of the changes in structural responses after the typhoon will be discussed in

the following section.

3.3. Integrity study of the OWT

3.3.1. Stochastic influences

The typhoon "In-fa" indeed induced strong fluctuation in structural responses as we discussed in Section 3.2. Consequentially, the impact of severe loads causes serious structural fatigue or even damage on the structure. Taking into account this fact, the study of the integrity influences induced by typhoon "In-fa" on the OWT structural responses has been carried out in this section. To identify the potential structure damage, the variation of the vibration intensity before and after the typhoon should be studied under the same external loads. As environmental loads such as the wind and waves, are typically distributed in the form of stochastic processes, the equivalent value of stochastic forces should be applied on the OWT to guarantee the same condition. To reflect this process, the four statistical wind loads and rotor speeds have been given in Table 6.

3.3.2. Integrity study

To investigate the impact of on OWT, the integrity study including the environmental and operational conditions has been conducted for the analysis under the above four statistical loads. In Fig. 18, it can be observed that the typhoon intensity gradually weakened and disappeared after July 29th. The wind speed was relatively lower than the value before or after the typhoon period. Most of the time, it rarely reached the rated speed and was slightly offset from the cut-in speed line. In practice, it is necessary to carry out an inspection of the OWT structure, timely maintain to avoid the potential fatigue or damage, and prevent safety accidents of the structure after the OWT structure has sustained extreme loads. Therefore, the structural response distribution and effective values before and after typhoon have been compared to investigate the influence of environmental loads on structural fatigue. Based on the aforementioned results, the ambient wind speed and rotor speed are considered the two most important factors affecting the structural response. **The comparison results of instantaneous amplitudes of acceleration and inclination under the same wind speed before and after the typhoon have been presented in Fig. 19.** The purpose of Fig. 19 is to confirm whether there are obvious variations or differences of structure response before and after the typhoon. The possible differences could indicate the characteristics for the evaluation of impactions on structural integrity by the typhoon. It has been noted that the slight change in structural acceleration under the same environmental and working conditions before and after the typhoon has occurred and the overall distributions has coincides

with each other, except for a few deviation points. Also, the RMS values of acceleration and inclination at the Level 1 and Level 5 have been provided before and after the typhoon. Throughout the comparison of all data, it has been concluded that the typhoon has caused great fluctuations of the marine environment and structural responses. While, the structural response can be restored to the original level (before the impact of the typhoon) when the typhoon passed. Currently, no obvious structural fatigue and damage have been observed by the data comparison. It has been suggested that the more specific and potential influence could be observed by continuous monitoring in the next few months. Also, the sustained strong wind resulted from the typhoon has greatly increased the power generation with additional economic benefits.

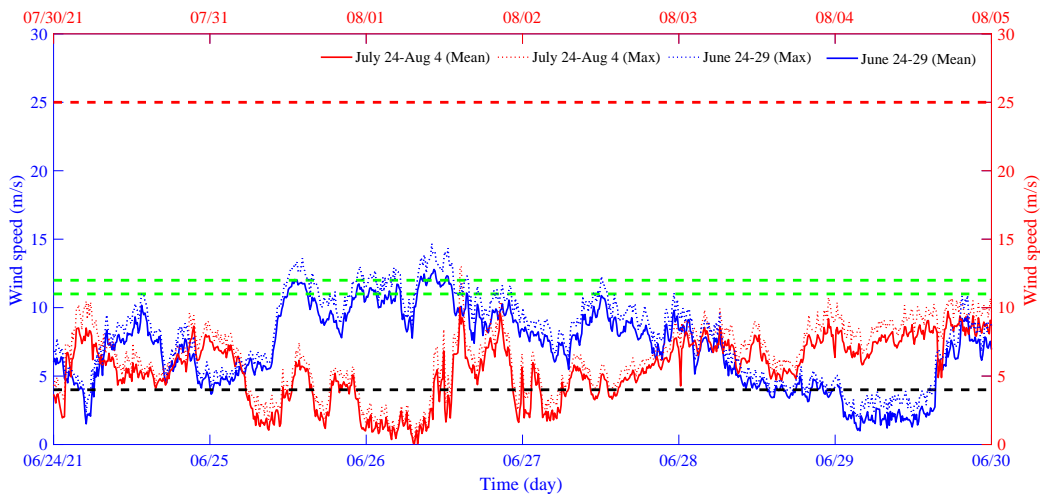


Fig. 18: Wind speed comparison of before and after the typhoon.

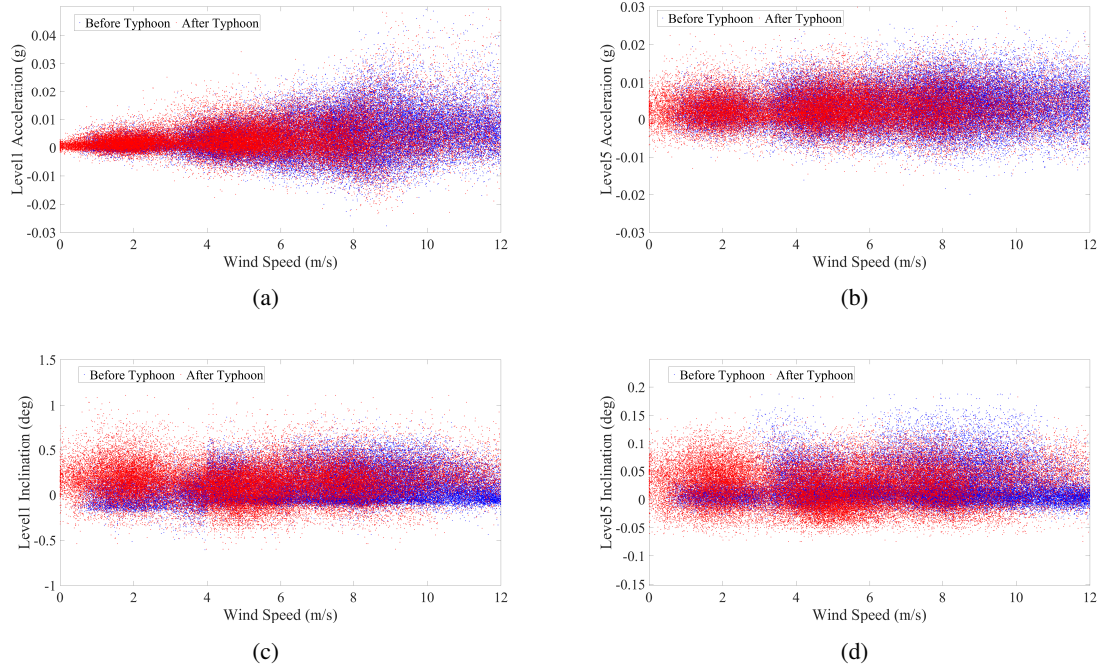


Fig. 19: Structural response comparison before and after typhoon: (a) Level 1 acceleration, (b) Level 5 acceleration, (c) Level 1 inclination, (d) Level 5 inclination.

Table 6: Structural response RMS before and after typhoon (June 24th-30th & August 15th-20th).

Wind speed (m/s)	Rotor speed (r/min)	Level 1 acceleration		Level 5 acceleration		Level 1 inclination		Level 5 inclination	
		RMS (g)		RMS (g)		RMS (deg)		RMS (deg)	
		Before typhoon	After typhoon	Before typhoon	After typhoon	Before typhoon	After typhoon	Before typhoon	After typhoon
<3	[0-1]	0.0023	0.0031	0.0040	0.0048	0.1654	0.2677	0.0149	0.0461
[4-6]	[3-7]	0.0045	0.0059	0.0054	0.0060	0.1830	0.2069	0.0354	0.0361
[6-10]	[7-10]	0.0079	0.0073	0.0066	0.0064	0.2148	0.2578	0.0450	0.0446
[11-12]	[10-12]	0.0105	0.0124	0.0068	0.0069	0.1452	0.2783	0.0244	0.0518

4. Potential applications of measured data

The proposed monitoring system obtains multi-source data, which should contain the in-depth information representing dynamic performances of OWT structures. Beyond data analysis conducted in Section

3, the potentials of multi-source data have been further demonstrated throughout three case studies as follows. Based on the explorations, two guide-lines have been concluded to assist the assessment of structural operational conditions.

4.1. Water depth estimation from the measured wave data

Water depth is an important parameter in the OWT monitoring. In practical applications, the water depth data of the OWT structure is usually obtained using a sounding rod, which can not realize the effective real-time online monitoring. Wave radar is one of the important components of the proposed system, it can not only measure the key characteristics of waves, but also estimate the water level depth through the measured real-time data and the parameters for example, the radar position and the measurement range shown in Fig. 3. Based on the reference data in Fig. 3, the water depth and tide can be estimated by Eqs. (1) and (2) using the radar measured value.

$$L_{water_depth} = M_{radar_measurement} + (H_{1985_benchmark} - (H_{radar_range} - H_{outer_platform})) \quad (1)$$

$$L_{tide_level} = M_{radar_measurement} - (H_{radar_range} - H_{out_platform}) \quad (2)$$

Due to scour or alluvium, the real mud line can not be obtained for the accurate calculation of the water depth. Therefore, in this paper the water depth has been estimated using Eq. (1). Fig. 20 shows the water depth estimation results before (in June) and during (in July) the typhoon. The maximum and average water depths on June and July are 10.09 m, 7.30 m and 10.97 m, 7.54 m, respectively. It has been noted that the water depth during the typhoon is up to 10.97 meters, with a remarkable increase as compared with the result in June. Therefore, it is necessary to make appropriate corrections to reflect the actual position of mud line in the long-term monitoring process.

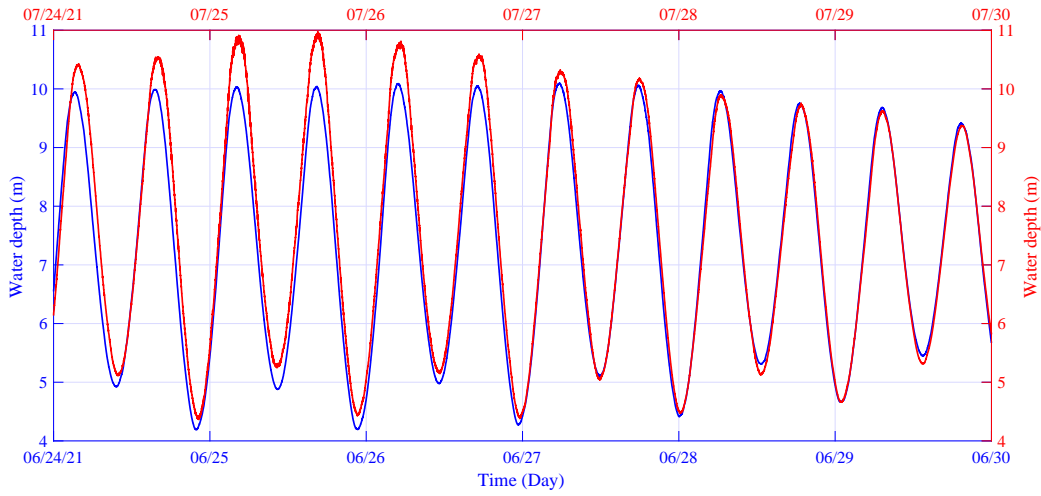


Fig. 20: Water depth estimation on June and July.

4.2. Intensity distribution of vibration along the tower

In Section 3, the effects of environmental factors including the wind speed and wind direction on OWT structural responses have been studied. In this section, the 12-day response changes of the OWT structure at different positions and directions under different wind speeds and directions before and during the typhoon will be analysed to determine the vibration amplitude and direction of the whole structure. Fig. 21 shows the correlation between the acceleration response and its synchronous wind speed on June 24th-29th. Obviously, a positive correlation between them can be observed and the amplitude on different levels varied alternately with different wind speeds. This phenomenon is particularly prominent at two intervals marked in the Fig. 21. In section #1, the wind speed is larger than 5 m/s and the section #2 is smaller than 5 m/s. However, the orders of magnitudes at five different levels are quite different. The zoomed sub-figures show the horizontal view (denoted in Fig. 2) of the acceleration for sections #1 and #2 at the five levels. In section #1, the most obvious feature is that the direction of the acceleration distribution at Level 1 is perpendicular to the vibration direction at other levels. In the x-axis direction, the acceleration amplitude at Level 3 is the largest, and in the y-axis direction, the maximum value of the acceleration amplitude at Level 1 can be observed. It is worth noting that in section #2, the acceleration amplitudes at the lower levels are larger than the value at the top level (Level 1), and the positions where the maximum acceleration amplitudes in two different directions locate, are also different.

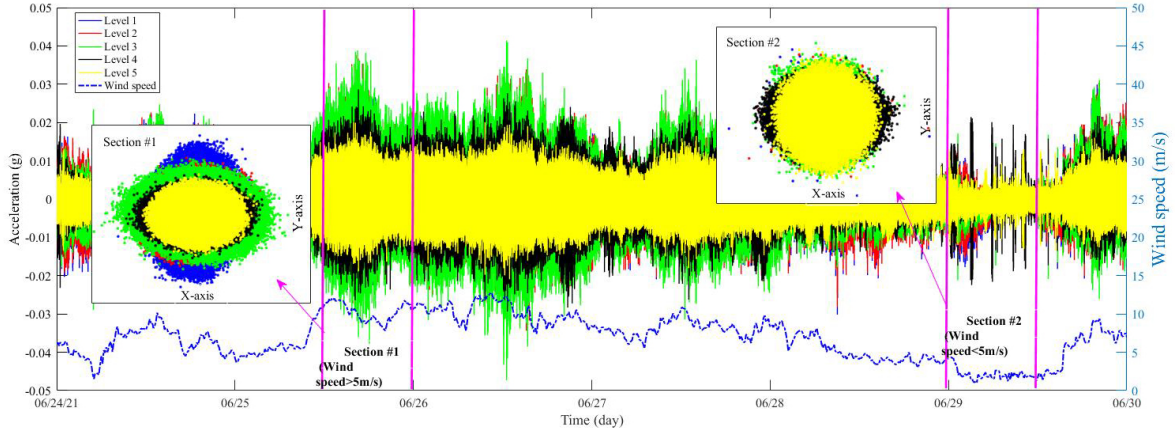


Fig. 21: Synchronized acceleration and wind speed on June 24th-29th.

To better understand the changes of the overall OWT structural responses under different environmental conditions, the analysis of structural responses at different positions and directions are statistically conducted. Assume that sensors are installed on the tower, where the global stationary coordinate is defined in Fig. 22a. It is necessary to apply a coordinate transformation to the collected signals so that the sensor data is represented along the nacelle orientation, which is defined by the fore-aft (FA) direction. The transform matrix is formulated by Eq. (3).

$$\begin{bmatrix} FA \\ SS \end{bmatrix} = \begin{bmatrix} \cos \theta & -\sin \theta \\ \sin \theta & \cos \theta \end{bmatrix} \cdot \begin{bmatrix} X_{axis} \\ Y_{axis} \end{bmatrix} \quad (3)$$

In Fig. 22a, the side-side (SS) is defined as the direction perpendicular to the FA direction. The angle between x-axis and FA direction is expressed as θ . And the direction of x-axis and y-axis are fixed at 45 degrees to the east and west respectively. With the coordinate transformation, the RMS values of structural acceleration along the wind speed in FA and SS directions are shown in Fig. 22b and c. In the FA direction, the change of the acceleration response at each level in respect to the wind speed is basically consistent with the results in Fig. 16, indicating the same process with four stages. It is noted that the RMS acceleration along the direction of SS does not gradually increase as with the wind speed increases. In the range of [0-5] m/s, the acceleration RMS increases with the increase of wind speed, and its maximum value is approximate to [6-7] m/s. In the range of [15-20] m/s, the RMS acceleration decreases with the increase of wind speed. However, the range of [10-15] m/s in Fig. 22c is denoted as the range for the rated wind speed and there is

a trough of the RMS acceleration indicating that the opposite trend is observed, as compared with the data in the FA direction.

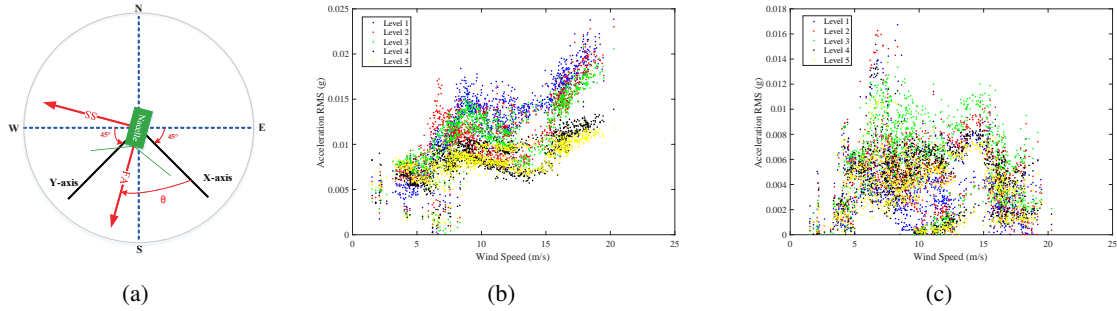


Fig. 22: Averaged acceleration RMS at five levels with wind speed: (a) coordinate transform, (b) FA, (c) SS.

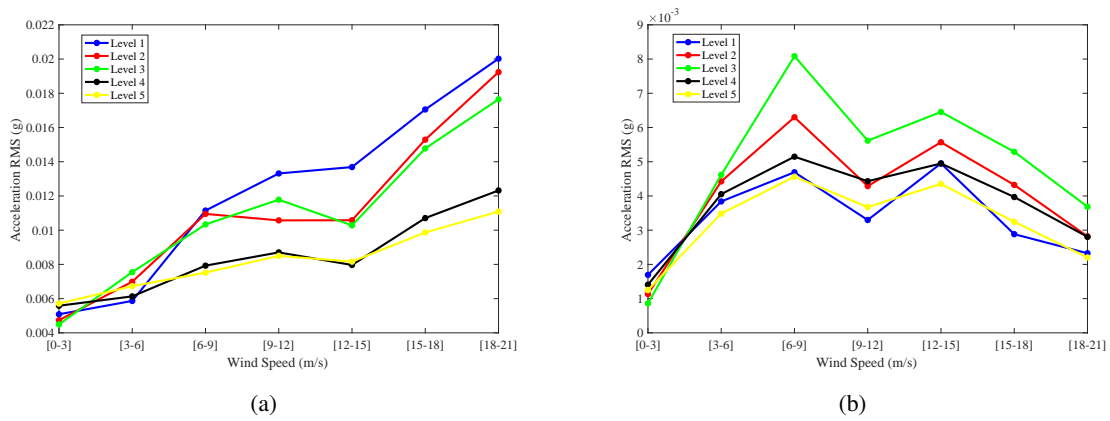


Fig. 23: Averaged acceleration RMS at five levels with wind speed: (a) FA, (b) SS.

Table 7: FA and SS comparison with wind speed.

	Wind Speed [m/s]						
	[0-3]	[3-6]	[6-9]	[9-12]	[12-15]	[15-18]	[18-21]
FA (RMS [g])	0.0051	0.0067	0.0096	0.0106	0.0101	0.0135	0.0161
SS (RMS [g])	0.0013	0.0041	0.0058	0.0043	0.0053	0.0039	0.0028

In order to explore the relationship among the acceleration amplitudes at different levels in the same range of the wind speeds, the discrete points have been evenly divided into seven wind intervals shown in Fig. 23. In the FA direction, when the wind speed is [0-3] m/s, the acceleration amplitude at the position

near the bottom of the tower is larger than the value at the top of the tower. As the wind speed is low, the main load of the OWT structure comes from waves and the vibration amplitude of the structure at the bottom is larger. Also, the similar conclusion can be drawn from the data arranged in the SS direction. In the range of [3-9] m/s, the acceleration of each layer in both FA and SS directions increases with the increase of the wind speed. The maximum vibration acceleration amplitude in the middle of the tower has been observed in both directions. When the wind speed is greater than 9 m/s, the vibration acceleration in the FA direction gradually increases along the tower. It is worth noting that in the SS direction, the acceleration amplitude in the middle of the tower remains the largest value in all positions, however the vibration amplitude at each level decreases with the increase of the wind speed. The comparison of mean values at all positions in FA and SS directions under different wind speeds has been shown in Table 7. It has been concluded that the average RMS acceleration in the FA direction is greater than the value in SS for seven ranges of wind speeds.

What's more, the resultant acceleration amplitude $A_{resultant}$ is calculated by Eq. (4) and shown in Fig. 24. The A_{FA} and A_{SS} are the acceleration RMS value from FA and SS direction respectively. The acceleration amplitude at each level of the OWT structure is linearly proportional to the wind speed. The change of acceleration amplitudes at different levels under different wind speeds is basically consistent with the trend illustrated in Fig. 23a and follows the principle: when the wind speed is in the range of [0-3] m/s, which represents the speed lower than the cut-in wind speed, the vibration intensity at the bottom (Level 5) of the structure is largest; When the wind speed is in the range of [3-9] m/s, the wind speed is greater than the cut-in wind speed, but lower than the rated wind speed. The maximal vibration intensity in the middle (Level 3) of the structure can be observed; When the wind speed is greater than the rated wind speed [10-11] m/s, the vibration intensity at the top of the tower has the largest value in the selected five positions.

$$A_{resultant} = \sqrt{A_{FA}^2 + A_{SS}^2} \quad (4)$$

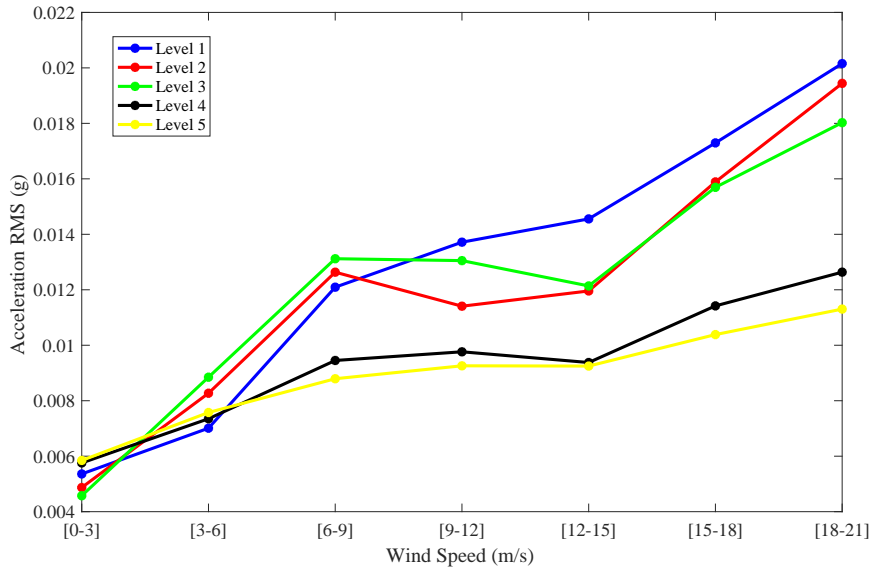


Fig. 24: Resultant acceleration RMS with wind speed.

Finally, the variations of vibration intensity distribution along with the wind speed were summarized to be the guideline #1. With the increment of wind speed from [0-3] m/s to [18-21] m/s, the largest vibration was changed from the bottom via the middle to the top position. When the wind speed is low, the major load comes from waves, tides and currents which forced on the bottom of the OWT structure. When the wind speed is increasing, the wind and operational loads are naturally getting prominent and the major load position is gradually transited from the bottom to the top regions. Based on the principle of dynamic responses, the guideline #1 could be mainly caused by changes of the load intensity and position on flexible tower structures. Meanwhile, the OWT structure investigated in our research is a representative entity and has been extensively installed in wind farms of China east coastal. And the long-term monitoring data includes structural information of OWTs subject to various operational conditions. Therefore, the guideline #1 could be considered a general conclusion for mono-pile OWT structures.

4.3. Frequency estimation from measured decay accelerations

Modal identification is one of the most important techniques for structural condition monitoring of OWTs. Due to the strong noisy signals caused by various environmental and operational conditions, modal parameters identification from ambient responses is a challenging task to be accurately achieved by operational modal analysis (OMA), especially for the damping ratio estimation. Traditional methods are usually based on the over-speed or rotor-stop test without the SCADA information, but they are not suitable for

the long-term monitoring. Therefore, how to accurately capture the attenuation response in the long-term monitoring process has become a hot research topic attracted with much attention.

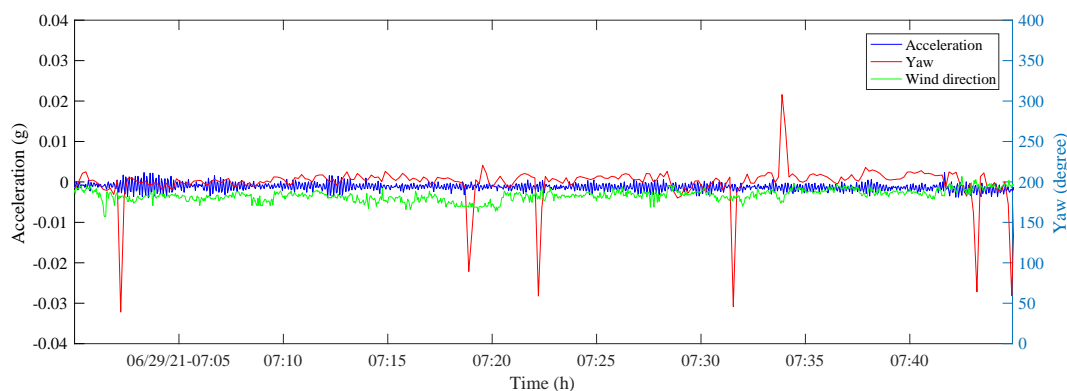


Fig. 25: Synchronization of yaw angle and acceleration.

As discussed in introduction, the nacelle yaw rigid-body motion may induce the strong vibration in the experimental test. The yaw and its synchronized acceleration at Level 1 have been presented in Fig. 25. As shown in Fig. 25, the large motion of nacelle ($> 100^\circ$) occurred seven times, and the maximum acceleration is 0.0023 g. It has been observed that the movements of nacelle just induce the small vibration without the expected decay progress (or free vibration response) which is used to identify the modal parameters [41]. This indicates that the identification accuracy of the resonance frequency and damping is not effectively improved by the vibration caused by the excitation force from the yaw rigid-body motion. In the long-term monitoring process, it is noted that different operational states have significantly affected vibrational responses of the OWT. In Fig. 26, six typical states including the operational (state 1 and 6), rotor-stop, parking, ship collision, and start-up, have been presented. Obviously, decay processes in ship collision (a and b) and rotor-stop (c) states can be used as crucial information to identify the frequency. In practice, the ship collision is seldom occurred and its relevant data can hardly be filtered from vibrational responses, while the rotor-stop can be recorded by the SCADA system in real-time and has the potential to the frequency identification in the long-term operational monitoring. The maximum acceleration value of the selected six states are 0.0355 g (operating: > 9 r/min), 0.0145 g (rotor-stop), 0.0035 g (parking), 0.0224 g (ship collision), 0.0149 g (start-up), 0.0121 g (operating: 3–9 r/min).

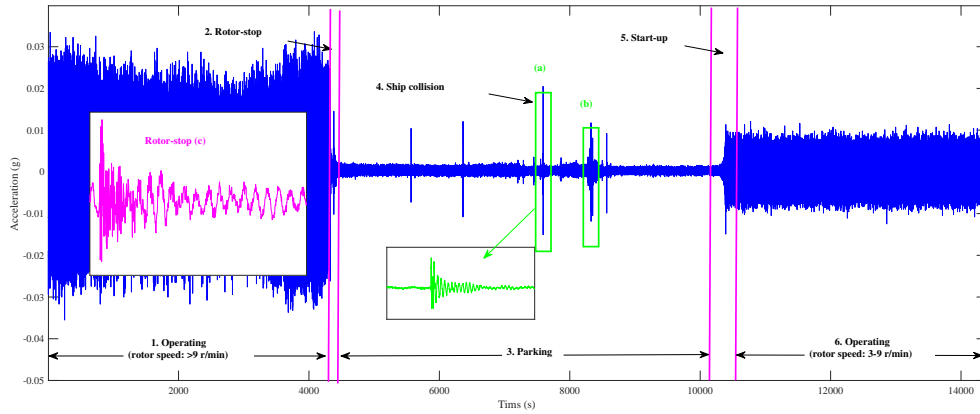


Fig. 26: Acceleration response in different operations.

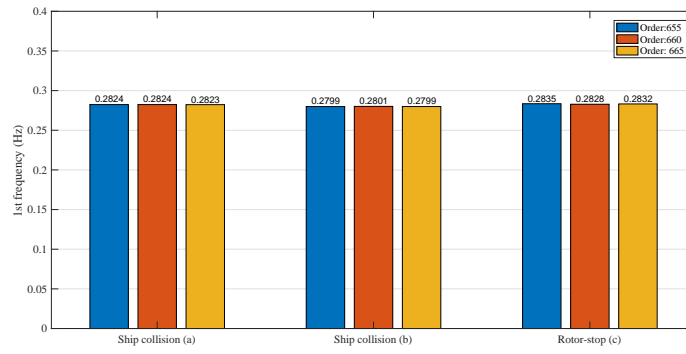


Fig. 27: Modal identification results.

To further validate the understanding of the aforementioned observations, the analysis has been performed using an eigensystem realization algorithm (ERA) method to estimate the modal frequency in use of two ship collision decays and one rotor-stop decay. In Fig. 27, the mean values of the first natural frequencies in these three decay processes are 0.2824 Hz, 0.2799 Hz and 0.2832 Hz, respectively. This proves that the data in the rotor-stop decay process can be applied for the long-term monitoring as the data in ship collision decay process does. Furthermore, to investigate the impact of the typhoon on the first frequency of OWT structures, a rotor-stop decay data on August 1th in Fig. 28 has been analysed. The maximum acceleration value in the selected rotor-stop process is 0.0125 g. The mean value of the 1st frequency after typhoon is 0.2824 Hz (order 655: 0.2827 Hz; order 660: 0.2821 Hz; order 665: 0.2824 Hz), which has agreed well with the result (0.2832 Hz) before typhoon in Fig. 27 rotor-stop (c). This is concluded that the typhoon has slight influence on the overall structural performance of the monitored OWT.

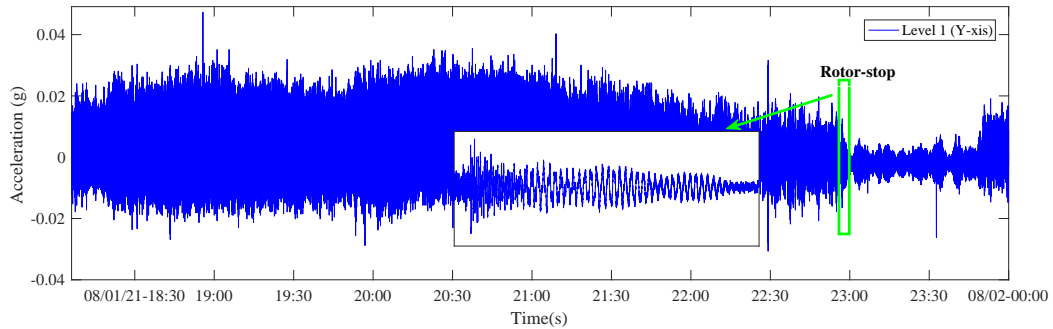


Fig. 28: Rotor-stop decay progress after the typhoon.

Finally, the above observations were summarized as the guideline #2 that the turbine rotor-stop and ship collision induced effective decay process for modal identification, but not the yaw rigid-body motion. The guideline # 2 was inspired by the researches [39–41] which found the decay acceleration data in the streaming data to assist the modal monitoring. And the rotor-stop and ship collision induced motions have been extensively used for the modal analysis of field OWT structural data[4, 46]. Therefore, this guideline is also believed to be a general conclusion.

5. Concluding Remarks

This paper presents a novel systematic study on structural performances of a 4.0 MW mono-pile OWT subject to typhoon "In-fa" using field-measured data. A real-time multi-source monitoring system, which has the ability to synchronously collect and analyse the data from waves, winds, vibrational accelerations and inclinations of towers, has been established for the evaluation on structural safety conditions and service life. It has been noted that during the typhoon period, the proportion of wave heights (more than 1.5 meters) has obviously increased and the tide level surpassing the design high tide level has reached 4.376 meters, but it has not exceeded the extreme level. Also, the acceleration and inclination amplitude have significantly increased, which were approximate 1.5-3 times of the previous records. Since the structural integrity characteristics have not been greatly affected, the OWT has successfully demonstrated its anti-typhoon ability. Moreover, the system has completely recorded the whole dynamic process of the typhoon and integrated the valuable data resources used for the operation monitoring of OWT under extreme loads. Throughout the data analysis and comparison, two guide-lines have been developed to facilitate the assessment of structural operational conditions. First, it is found that the rotor-stop process will lead to the decay response, which provides reliable data for the accurate identification of modal parameters including the damping ratio for the

long-term monitoring; Second, the position of the most serious vibration is not always near the turbine, but it changes along with the wind speed. In particular, the change in the position where the maximum structural response is represented varies in two directions (FA and SS), whilst the magnitude of the vibration response in the FA direction is always larger than the value in the SS direction. This observation indicates that the structural safety can be assessed if the change in the position of the maximum structural response is different from the prediction under the same wind speed. With the aforementioned contributions, there is an opportunity to provide engineers and designers with valuable information for the long-term monitoring and optimization of OWT and cost reduction of renewable energy exploitation in the future.

6. Declaration of competing interest

The authors declare that they have no known competing financial interests or personal relationships that could have appeared to influence the work reported in this paper.

7. Acknowledgements

The authors acknowledge the financial support of the National Natural Science Foundation-Basic Science Center Project (52088102) and the National Outstanding Youth Science Fund Project of National Natural Science Foundation of China (52125106). Thanks to China Green Development Group, Rudong offshore wind farm in Jiangsu Province and Power China Huadong Engineering Corporation Limited, for their strong support on the field monitoring system test in this paper.

References

- [1] D. Xu, X. Xu, W. Li, B. Fatahi, Field experiments on laterally loaded piles for an offshore wind farm, *Marine Structures* 69 (2020) 102684. doi:10.1016/j.marstruc.2019.102684.
- [2] X. Dong, J. Lian, H. Wang, Vibration source features of offshore wind power structures under operational conditions, *Journal of Vibration and Shock* 36 (17) (2017) 21–28.
- [3] F. Liu, S. Gao, S. Chang, Displacement estimation from measured acceleration for fixed offshore structures, *Applied Ocean Research* 113 (4) (2021) 102741. doi:10.1016/j.apor.2021.102741.
- [4] L. Zhou, Y. Li, F. Liu, Z. Jiang, Q. Yu, L. Liu, Investigation of dynamic characteristics of a monopile wind turbine based on sea test, *Ocean Engineering* 189 (2019) 106308.1–106308.17. doi:10.1016/j.oceaneng.2019.106308.
- [5] M. El-Kafafy, G. D. Sitter, C. Devriendt, W. Weijtjens, Monitoring resonant frequencies and damping values of an offshore wind turbine in parked conditions, *Renewable Power Generation Let* 8 (4) (2014) 433–441. doi:10.1049/iet-rpg.2013.0229.

- [6] F. Liu, H. Li, H. Lu, Weak-mode identification and time-series reconstruction from high-level noisy measured data of offshore structures, *Applied Ocean Research* 56 (2016) 92–106. doi:10.1016/j.apor.2016.01.001.
- [7] S. Wang, H. Han, F. Liu, W. Li, S. Gao, Transfer path analysis for semisubmersible platforms based on noisy measured data, *Energies* 12 (24) (2019) 4801. doi:10.3390/en12244801.
- [8] B. Puruncas, Y. Vidal, C. Tutivn, Vibration-response-only structural health monitoring for offshore wind turbine jacket foundations via convolutional neural networks, *Sensors* 20 (12) (2020) 3429. doi:10.3390/s20123429.
- [9] T. Moan, Z. Gao, E. E. Bachynski, A. R. Nejad, Recent advances in integrated response analysis of floating wind turbines in a reliability perspective, *Journal of Offshore Mechanics and Arctic Engineering* 142 (5) (2020) 1–73. doi:10.1115/1.4046196.
- [10] J. Zhang, H. Lu, K. Sun, Dynamic response analysis for offshore structures by a combination of segmented responses based on pole-residue method, *Ocean Engineering* 219 (1) (2020) 108277. doi:10.1016/j.oceaneng.2020.108277.
- [11] W. Hu, T. Sebastian, R. G. Rohrman, S. Said, W. Ruecker, Vibration-based structural health monitoring of a wind turbine system part ii: Environmental/operational effects on dynamic properties, *Engineering Structures* 89 (2015) 273–290. doi:10.1016/j.engstruct.2014.12.035.
- [12] W. Hu, T. Sebastian, R. G. Rohrman, S. Said, W. Ruecker, Vibration-based structural health monitoring of a wind turbine system. part i: Resonance phenomenon, *Engineering Structures* 89 (2015) 260–272. doi:10.1016/j.engstruct.2014.12.034.
- [13] W. Weijtjens, T. Verbelen, G. De Sitter, C. Devriendt, Foundation structural health monitoring of an offshore wind turbine—a full-scale case study, *Structural Health Monitoring: An International Journal* 15 (4) (2016) 389–402. doi:10.1177/1475921715586624.
- [14] F. Liu, S. Gao, D. Liu, H. Zhou, A signal decomposition method based on repeated extraction of maximum energy component for offshore structures, *Marine Structures* 72 (15) (2020) 260–272. doi:10.1016/j.marstruc.2020.102779.
- [15] Summary of wind turbine accident, Date to 31 december 2021. [Http://www.caithnesswindfarms.co.uk/AccidentStatistics.htm](http://www.caithnesswindfarms.co.uk/AccidentStatistics.htm) (accessed on 25 February 2021).
- [16] T. Ishihara, A. Yamaguchi, K. Takahara, T. Mekar, S. Matsuura, An analysis of damaged wind turbines by typhoon maemi in 2003, in: *The Sixth Asia-Pacific Conference on Wind Engineering*, 2005.
- [17] J. Li, Z. Li, Y. Jiang, Y. Tang, Typhoon resistance analysis of offshore wind turbines: A review, *Atmosphere* 13 (2022) 451. doi:10.3390/atmos13030451.
- [18] J. Lian, Y. Jia, H. Wang, Numerical simulation for characteristics of wind loads of 2.5mw wind turbine under typhoon, *Acta Energiae Solaris Sinica* 39 (3) (2018) 611–618.
- [19] Z. Wang, B. Zhang, Y. Zhao, G. Liu, J. Jiang, Danamic response of wind turbine under typhoon, *Acta Energiae Solaris Sinica* 34 (8) (2013) 1434–1442.
- [20] X. Zhang, M. Wang, Y. Wang, Y. Liu, Research on failure of offshore wind turbine tower in typhoon, 2018 OCEANS - MTS/IEEE Kobe Techno-Oceans (OTO) (2018) 1–4doi:10.1109/OCEANSKOBE.2018.8559456.
- [21] W. Bao, H. Wang, S. Ke, Typhoon-induced response characteristics and yaw effects of large wind turbine based on multi-body dynamics method, *Jouranal of Vibration and Shock* 39 (15) (2020) 257–265.
- [22] T. Fan, S. Chen, C. Huang, Strength analysis for a jacket-type substructure of an offshore wind turbine under extreme environment conditions, *International Journal of Offshore and Polar Engineering* 30 (4) (2020) 414–420. doi:10.17736/

ijope.2020.ty07.

- [23] J. Li, J. Bian, Y. Ma, Y. Jiang, Impact of typhoons on floating offshore wind turbines: A case study of typhoon mangkhut, *Journal of Marine Science and Engineering* 9 (5) (2021) 543. doi:10.3390/jmse9050543.
- [24] X. Lu, S. Ke, Wind vibration response analysis of large wind turbine system considering stopping position under meso-micro scale, *Journal of Vibration and Shock* 39 (1) (2020) 91–101. doi:10.13465/j.cnki.jvvs.2017.07.014.
- [25] H. Wang, S. Ke, T. Wang, S. Zhu, Typhoon-induced vibration response and the working mechanism of large wind turbine considering multi-stage effects, *Renewable Energy* 153 (2020) 740–758. doi:10.1016/j.renene.2020.02.013.
- [26] K. Tanaka, T. Utsunomiya, I. Sato, H. Kakuya, Comparison of dynamic response in a 2mw floating offshore wind turbine during typhoon approaches, *ASME International Conference on Ocean*.
- [27] Z. Li, S. Chen, H. Ma, T. Feng, Design defect of wind turbine operating in typhoon activity zone, *Engineering Failure Analysis* 27 (2013) 165–172. doi:10.1016/j.engfailanal.2012.08.013.
- [28] X. Chen, J. Xu, Structural failure analysis of wind turbines impacted by super typhoon usagi, *Engineering Failure Analysis* 60 (2016) 391–404. doi:10.1016/j.engfailanal.2015.11.028.
- [29] X. Chen, C. Li, J. Xu, Failure investigation on a coastal wind farm damaged by super typhoon: A forensic engineering study, *Journal of Wind Engineering and Industrial Aerodynamics* 1417 (2015) 132–142. doi:10.1016/j.jweia.2015.10.007.
- [30] W. Tang, Q. Yuan, Z. Han, With standing typhoon design of wind turbine tower, *Acta Energiæ Solaris Sinica* 29 (4) (2008) 422–427. doi:10.3321/j.issn:0254-0096.2008.04.009.
- [31] S. Chi, C. Liu, C. Tan, Y. Chen, Study of typhoon impacts on the foundation design of offshore wind turbines in taiwan, *Proceedings of the Institution of Civil Engineers - Forensic Engineering* 173 (1) (2020) 35–47. doi:10.1680/jfoen.19.00011.
URL <https://doi.org/10.1680/jfoen.19.00011>
- [32] T. Lin, Y. Qumner, Extreme typhoon loads effect on the structural response of offshore meteorological mast and wind turbine, *Proceedings of 7th PAAMES and AMEC2016* 6. doi:10.1115/OMAE2016-55008.
- [33] B. Nelson, T. Lin, Y. Qumner, H. Huang, C. Chien, Extreme typhoon loads effect on the structural response of an offshore wind turbine, *Proceedings of 7th PAAMES and AMEC2016*.
- [34] J. Li, W. Wu, Y. Wei, Y. Shu, Z. Lu, W. Lai, P. Jia, Z. Cheng, Y. Xie, Study on dynamic response of offshore wind turbine structure under typhoon, *Polish Maritime Research* 29 (2022) 34–42. doi:10.2478/pomr-2022-0004.
- [35] G. Huang, X. Zhao, C. Zhou, K. Wei, F. Wu, S. Zhang, Improved wind-induced fragility assessment method of offshore wind turbines under typhoon and its application, *Journal of Vibration Engineering* 35 (2) (2022) 331.
- [36] M. Qin, W. Shi, W. Chai, X. Fu, X. Li, Research on dynamic characteristics of large-scale monopile offshore wind turbine under typhoon event, *Chinese Journal of Theoretical and Applied Mechanics* 54 (4) (2022) 881–891.
- [37] X. Sun, S. Cao, C. Yan, Z. Zhu, Monitoring typhoon-induced vibration and tilt of offshore wind turbine system for batholith seabed, *International Journal of Offshore and Polar Engineering* 29 (1) (2019) 8–14. doi:10.17736/ijope.2019.1152.
- [38] X. Dong, J. Lian, H. Wang, Monitoring experiment and characteristic analysis of structural vibration of offshore wind turbine, *Journal of Tianjin University Science and Technology* (2019).doi:10.11784/tdxbz201708007.
- [39] X. He, Q. He, B. Jin, T. Zheng, Vibration characteristics of multi-pile-concrete wind turbine towers, *Journal of Vibration and*

Shock 38 (19) (2019) 174–181.

- [40] Z. Yi, B. Jin, T. Zheng, Strong vibration analysis of single-pile foundation offshore wind power tower, *South China Journal of Seismology* 40 (04) (2020) 133–139.
- [41] W. Deng, B. Jin, T. Zheng, Analysis of vibration characteristics of high-pile at sea-concrete offshore wind turbine tower, *Earthquake Engineering and Engineering Dynamics* 40 (01) (2020) 233–241.
- [42] Guidelines for structure health monitoring for offshore wind turbine tower and foundations. <https://www.ngi.no/eng/publications-and-library> (accessed on 13 august 2021).
- [43] Global wind energy council. global wind statistics 2021. global statistics. 2021. <http://gwec.net/> (accessed on 18 august 2021).
- [44] S. Yu, D. Zhang, S. Wang, G. Wang, G. Li, Field monitoring of offshore wind turbine foundations in ice regions, *Journal of Coastal Research* 104 (2020) 343–350. doi:10.2112/JCR-SI104-063.1.
- [45] Zoom Earth, <https://zoom.earth/storms/in-fa-2021/#map=daily/overlays=fires> (2021).
- [46] M. Damgaard, L. B. Ibsen, L. V. Andersen, J. Andersen, Cross-wind modal properties of offshore wind turbines identified by full scale testing, *Journal of Wind Engineering and Industrial Aerodynamics* 116 (2013) 94–108. doi:10.1016/j.jweia.2013.03.003.

Appendix

Table A1: Wind Turbine Accident and Incident Compilation with Typhoon/Hurricane.

No	Accident type	Date	Site/area	Country	Turbine type
1	Structural failure	26/12/1998	Owenreagh, County Tyrone Northern Ireland	UK	-
2	Structural failure	Sept-1999	-	Japan	-
3	Structural failure	11/09/2003	Miyakojima Island	Japan	Micon M750/400kW Enercon E40/500kW
4	Structural failure	2003	Honghai Bay wind works	China	-
5	Blade failure	20/01/2005	Various	Denmark	-
6	Structural failure	15/08/2006	Hedingshan wind farm in East China's Zhejiang Province	China	-
7	Structural failure	15/08/2006	Cangnan Wind Farm	China	-
8	Transport	19/09/2007	Beaumont, Texas	USA	-
9	Structural failure	25/10/2008	Gruti Field hill Voe, Shetland	UK	-
10	Blade failure Structural failure	25/09/2013	Honghaiwan wind farm Shanwei City, Guangdong	China	Vestas V47
11	Structural failure	12/08/2015	Taichung wind farm	Taiwan	-
12	Structural failure	12/08/2015	Shihmen District New Taipei, Taiwan	Taiwan	-
13	Miscellaneous	31/05/2017	Awaji Island Hyogo Prefecture	Japan	-
14	Structural failure	24/08/2018	Awaji Island Hyogo Prefecture	Japan	-
15	Blade failure	09/03/2019	Freckleben Aschersleben Salzlandkreis	Germany	DeWind D6/62
16	Structural failure	02/06/2020	Medicine Hat College, Alberta	Canada	-
17	Structural failure	05/11/2020	Satec floating wind turbine, Bilbao	Spain	-

*Last updated at 05/07/2021, compiled by CWIF